frontiers | Frontiers in Materials

TYPE Original Research
PUBLISHED 24 April 2023
DOI 10.3389/fmats.2023.1187094

OPEN ACCESS

EDITED BY
Pshtiwan Shakor,
Institute of Construction Materials, Australia

REVIEWED BY
Muhammad Javed,
COMSATS Institute of Information Technology, Pakistan
M. Aminul Haque,
Hong Kong Polytechnic University, Hong Kong SAR, China

*CORRESPONDENCE
Gongmei Chen,
drgongmeichen@outlook.com
Alireza Bahrami,
Alireza.Bahrami@hig.se

SPECIALTY SECTION
This article was submitted to Structural Materials, a section of the journal Frontiers in Materials

RECEIVED 15 March 2023
ACCEPTED 27 March 2023
PUBLISHED 24 April 2023

CITATION
Chen G, Suhail SA, Bahrami A, Sufian M and Azab M (2023), Machine learning-based evaluation of parameters of high-strength concrete and raw material interaction at elevated temperatures. *Front. Mater.* 10:1187094. doi: 10.3389/fmats.2023.1187094

Machine learning-based evaluation of parameters of high-strength concrete and raw material interaction at elevated temperatures

Gongmei Chen[1]*, Salman Ali Suhail[2], Alireza Bahrami[3]*, Muhammad Sufian[4] and Marc Azab[5]

[1]School of Architecture and Civil Engineering, Changchun Sci-Tech University, Changchun, China, [2]Department of Civil Engineering, University of Lahore (UOL), Lahore, Pakistan, [3]Department of Building Engineering, Energy Systems and Sustainability Science, Faculty of Engineering and Sustainable Development, University of Gävle, Gävle, Sweden, [4]School of Civil Engineering, Southeast University, Nanjing, China, [5]College of Engineering and Technology, American University of the Middle East, Egaila, Kuwait

High-strength concrete (HSC) is vulnerable to strength loss when exposed to high temperatures or fire, risking the structural integrity of buildings and critical infrastructures. Predicting the compressive strength of HSC under high-temperature conditions is crucial for safety. Machine learning (ML) techniques have emerged as a powerful tool for predicting concrete properties. Accurate prediction of the compressive strength of HSC is important as HSC can experience strength losses of up to 80% after exposure to temperatures of 800°C–1000°C. This study evaluates the efficacy of ML techniques such as Extreme Gradient Boosting, Random Forest (RF), and Adaptive Boosting for predicting the compressive strength of HSC. The results of this study demonstrate that the RF model is the most efficient for predicting the compressive strength of HSC, exhibiting the R^2 value of 0.98 and lower mean absolute error and root mean square error values than the other applied models. Furthermore, Shapley Additive Explanations analysis highlights temperature as the most significant factor influencing the compressive strength of HSC. This article provides valuable insights into the timely and effective determination of the compressive strength of HSC under high-temperature conditions, benefiting both the construction industry and academia. By leveraging ML techniques and considering the critical factors that influence the compressive strength of HSC, it is possible to optimize the design and construction process of HSC and enhance its resilience to high-temperature exposure.

KEYWORDS

compressive strength, high-strength concrete, machine learning, raw material interaction, fire resistance

1 Introduction

In recent years, the construction sector has developed considerable interest in using high-strength concrete (HSC) for applications like high-rise buildings, offshore structures, and bridges. The primary utilization of HSC in buildings is structural framing, including columns and beams that are major load-bearers. Therefore, adequate measures against fire safety are vital safety prerequisites in building design. With enhanced applications of HSC, there is rising concern about HSC's behavior in fire, which can damage structures (Figure 1). The phenomenon of spalling at higher temperatures is the primary reason for this concern (Khaliq and Kodur, 2018; Xiong and Liew, 2020; Kushnir et al., 2021; Lalu et al., 2021; Li et al., 2021). Usually, the structural elements of normal-strength concrete show considerable performance under exposure to fire. However, a distinct difference is reported in the literature between HSC and normal-strength concrete after exposure to fire (Bilodeau et al., 2004; Laneyrie et al., 2016; Ozawa et al., 2017; Cao et al., 2018). Moreover, the explosive spalling that occurs in HSC under exposure to rapid fire is also of significant concern (Alfahdawi et al., 2019; Xiong and Liew, 2020; Afzal and Khushnood, 2021; Li et al., 2021; Khan et al., 2022c). The HSC's fire response tracing demands the application of precise modeling which can adequately account for the HSC's structural response and material properties like spalling on exposure to real fire scenarios. This rising concern about the HSC's behavior in fire requires adequate fire safety measures and the application of precise modeling that can account for the HSC's structural response and material properties upon exposure to real fire scenarios.

The development of HSC in the cementitious material field occurred between the 1950s and 1960s, and its compressive strength was designated over 40 MPa (Carrasquillo et al., 1981). HSC has very little impermeability, high density, and high durability, making for wide application in the construction sector in skyscrapers, long-span bridges, and piers. The design method of HSC is comparatively more complex than standard strength concrete, demanding in-depth knowledge of the mechanical and chemical characteristics of its ingredients, more experience, and multiple trials to attain concrete of the required properties. One of the key factors in the design of HSC structures is the compressive strength (Duan et al., 2013). Deficiency in the compressive strength of HSC may result in severe structural failures and difficult repairs, as HSC is primarily designed to bear excessive compressive forces (Al-Shamiri et al., 2019). Incorporation of different materials such as fibers (Xie et al., 2021; Shi et al., 2022; Sun et al., 2023), hinges (Huang et al., 2022; Huang et al., 2023a), and special cements (Wang et al., 2022) has also been reported to enhance the properties of cementitious composites. Moreover, researchers are more attentive nowadays to sustainable supplementary cementitious materials for sustainable development (Cao et al., 2019; Arshad et al., 2020; Khan et al., 2021; Ahmad et al., 2023; Lao et al., 2023a; Lao et al., 2023b; Qian et al., 2023; Riaz Ahmad et al., 2023). The timely and precise determination of the compressive strength of HSC can save costs and time, as it is the requirement of various design standards and codes. The complexity of HSC structures requires significant expertise, and accurate determination of the compressive strength is crucial to prevent structural failure.

FIGURE 1
Fire consequences (Wróblewski and Stawiski, 2020).

Applying machine learning (ML) approaches can effectively solve complex issues in different engineering fields (Dong et al., 2023b; Huang et al., 2023b). ML approaches can predict the output depending on the input variable dataset (Huang et al., 2021; Wang et al., 2022; Zhang et al., 2023). Both individual and ensemble ML approaches are employed. The Decision Tree (DT) is classified as an individual approach, whereas the Random Forest (RF), eXtreme Gradient Boosting (XGBoost), and Adaptive Boosting (AdaBoost) are categorized as ensemble ML techniques. It has been frequently reported in the literature that ensemble ML approaches tend to perform better than individual ones, possibly due to the ability of ensembles to reduce the variance and bias of individual models, capture a broader range of patterns and relationships within the data, and improve generalization to new and unseen examples. Ensembles can also be useful in cases where individual models are prone to overfitting or have limitations in their predictive capacity. Overall, ensemble approaches have become increasingly popular in ML due to their potential to increase prediction accuracy and robustness and their versatility for use across different application domains (Wang et al., 2022). ML techniques are used to investigate the mechanical properties of concrete (Chaabene et al., 2020; Khan et al., 2022d). Additionally, research works were conducted on multiple types of concrete, such as phase change material-integrated concrete (Marani and Nehdi, 2020), high-performance concrete (HPC) (Castelli et al., 2013), recycled aggregate concrete (RAC) (Zhang et al., 2020), and self-healing concrete (Ramadan Suleiman and Nehdi, 2017), to estimate their characteristics. Han et al. (2019) utilized ML techniques to predict the compressive strength of HPC by considering various parameters such as cement, aggregates, sand, water, ground granulated blast-furnace slag, and age. Their algorithm achieved high accuracy in the HPC's strength estimation. ML approaches, especially ensemble techniques, have been increasingly applied to solve complex issues and improve prediction accuracy and robustness in various engineering fields, including the investigation of mechanical properties of different types of concrete; further research is needed to explore the effects of fire exposure on the HSC's performance and its interactions with various parameters.

The mechanical characteristics of HSC have been extensively evaluated in numerous studies. However, the laboratory processes

for casting, curing, and testing specimens require considerable effort, time, and cost. Hence, applying ML, such as advanced approaches, for assessing the characteristics of HSC may solve these issues and decrease experimentation costs (Dong et al., 2023a; Asghari et al., 2023; Sami et al., 2023). Accordingly, this research applies three different ensemble ML approaches—XGBoost, Adaboost, and RF—for the compressive strength prediction of HSC. These ensemble algorithms are better than individual algorithms for predicting the compressive strength of HSC at high temperatures (Ahmad et al., 2021). For predicting the compressive strength of HSC *via* the application of ML algorithms, the considered input parameters include cement (kg/m^3), fly ash (kg/m^3), nano-silica (kg/m^3), water (kg/m^3), super plasticizer (kg/m^3), fine and coarse aggregates (kg/m^3), silica fume (kg/m^3), and temperature (°C). These parameters are taken as predictor variables for the compressive strength of HSC. Moreover, the employed algorithms' performance is also evaluated with the help of comparison and statistical analysis. Depending on the evaluated performance, a better algorithm is recommended to determine the strength of HSC. Furthermore, the basic constituents' influence on the strength of HSC is yet to be explored. Thus, the influence of HSC's raw ingredients—the input parameters—on the strength under compressive loading—its output parameter—is evaluated and explained in detail by Shapley Additive Explanations (SHAP) analysis. The integration of SHAP with the utilized ML models will gain detailed information on HSC mix design with respect to its strength parameters through complex non-linear behavior. It will aid in developing sustainable and fire-resistant HSC mixes.

2 Research significance

The manufacturing and testing of HSC for evaluating its superior properties involve costly and time-consuming laboratory procedures such as specimen casting, curing, and testing. Modern ML techniques have recently been employed to tackle these challenges in predicting the mechanical behavior of HSC. This study utilizes ensemble ML approaches—including XGBoost, Adaboost, and RF—to predict the compressive strength of HSC. It investigates the effect and interaction of raw ingredients through the SHAP analysis, using nine input factors as predictor variables. The models are executed using Python programming language, and k-fold cross-validation is utilized to verify test data. The SHAP analysis is used to examine the contribution of each input factor to the compressive strength of HSC. The study aims to enhance the efficiency, effectiveness, and cost-effectiveness of designing fire-resistant structures and can serve as a foundation for future HSC research at high temperatures.

3 Standard machine learning models

3.1 Extreme Gradient Boosting (XGBoost) algorithm

An XGBoost model is a reliable tool for scientists in the data science field because of an efficient ensemble tree-based model (Chen and Guestrin, 2016). The structure of Adaboost, which employs various functions for predicting the output by Eq. 1, is the base of Extreme Adaboost (Friedman, 2001).

$$\bar{y}_i = y_i^0 + \eta \sum_{K=1}^{n} f_k(U_i) \tag{1}$$

Here, the predicted outcome is demonstrated by $\bar{y}_i$ having *i*th data with U_i, which is a variable vector; n denotes the number of predictors as per independent tree structures for each f_k (k = 1-n); y_i^0 is the primary hypothesis; η denotes the learning rate to increase the algorithm's performance and connect supplementary trees to avoid overfitting. The main limitation of ML is developing a model with minimum overfitting. In XGBoost, the complementary evaluation of the training phase is done.

According to Eq. 1, on the *k*th level, the *k*th predictor is linked with the algorithm and *k*th y_i^{-k} prediction is evaluated by the estimated outcome $y_i^{-(k-1)}$ in the subsequent phase. The established f_k for the *k*th predictor is given in Eq. 2.

$$y_i^{-k} = y_i^{-(k-1)} + \eta f_k \tag{2}$$

f_k denotes the weight of the leaves, established by limiting the objective function of the *k*th tree (Eq. 3).

$$f_{obj} = \gamma Z + \sum_{a=1}^{Z} \left[g_a \omega_a + \frac{1}{2} (h_a + \lambda) \omega_a^2 \right] \tag{3}$$

Here, the leaf nodes' quantum is depicted by Z, the constant coefficient by λ, the factor of complexity by c, and leaf weight (1—Z) by ω_a^2. c and λ are the governing parameters employed for improving the model in order to avoid over-fitting; g_a and h_a are the summed parameters against the entire database connected with the gradient leaf of the initial and previous loss function, respectively. To build the *k*th tree, a leaf is additionally distributed in various leaves. The gain factors are utilized to apply this system, provided in Eq. 4.

$$G = \frac{1}{2} \left[\frac{O_L^2}{P_L + \lambda} + \frac{O_R^2}{P_R + \lambda} + \frac{(O_L + O_R)^2}{P_L + P_R + \lambda} \right] \tag{4}$$

The gain factors are represented with G, left and right leaf, P_L and O_L, and P_R and O_R. The standards for division are usually supposed during the approximation of the gain factor toward '0'. c and λ are governing parameters indirectly based on gain factors. For example, the gain factor may be significantly reduced with a greater regularization factor, ultimately avoiding the convolution process of a leaf. However, in this case, the model's performance in selecting the training data can also be decreased. The XGBoost basic step-wise structure is presented in Figure 2.

3.2 Adaptive Boosting (Adaboost) algorithm

One of the supervised ML approaches is the AdaBoost Regressor, which utilizes an ensemble technique. This approach involves reallocation of weights for each instance, where higher weights are assigned to those that have been incorrectly identified. These techniques are typically employed in supervised learning to reduce bias and variance and improve the performance of weak learners. Furthermore, this approach uses bulk quantities of DTs during data training. The mistakenly characterized recorded data are assigned a high priority weight for developing the initial model/

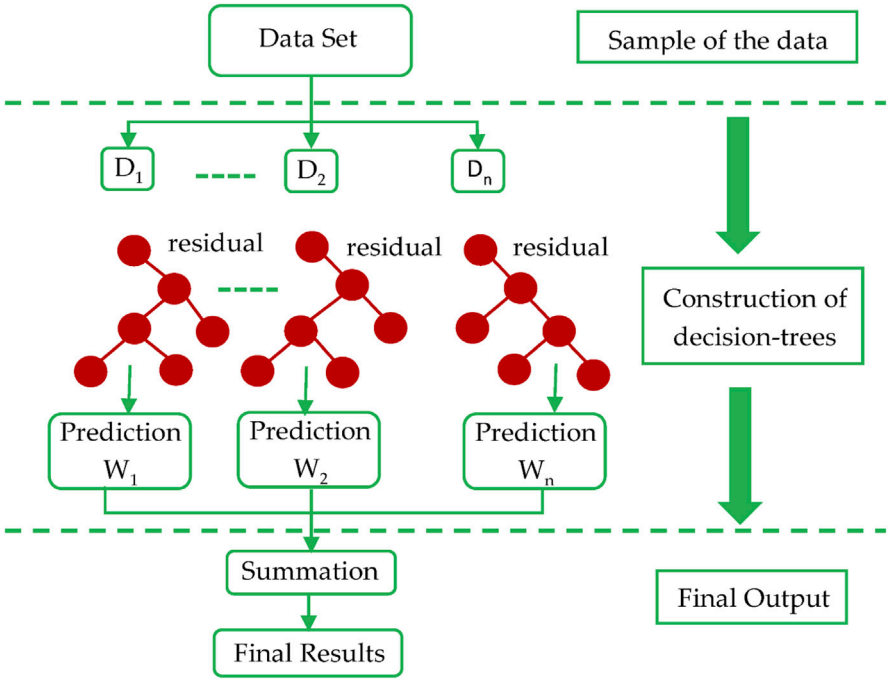

FIGURE 2
Structure of the XGBoost algorithm (Amjad et al., 2022).

DT. These data entries are selected as input for the other algorithms. This process is repeated until the desired quantity of basic learners is fulfilled. In terms of binary classification issues, AdaBoost is better at enhancing the performance of DT and may be applied to boost the efficacy of ML techniques. The Adaboost basic step-wise structure is shown in Figure 3.

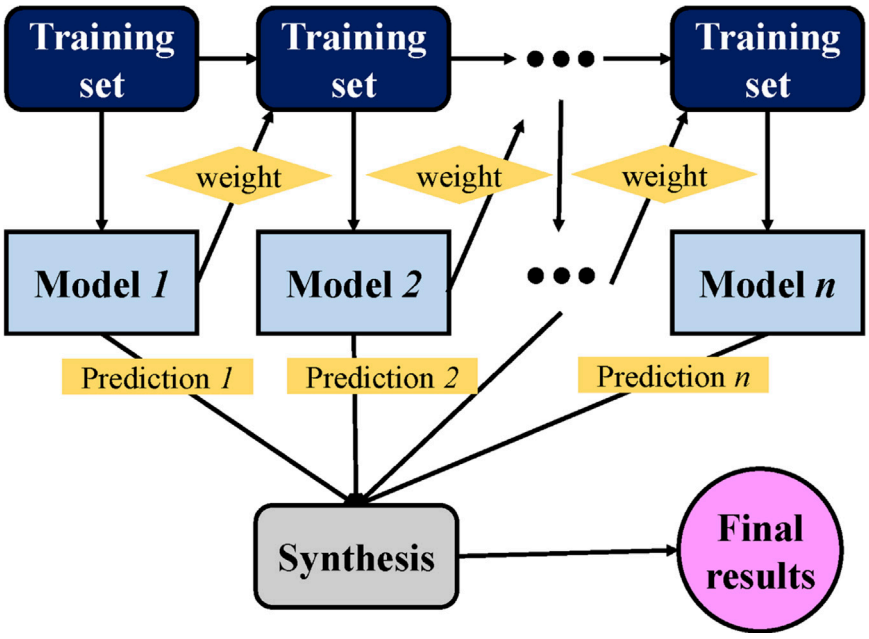

FIGURE 3
Structure of the Adaboost algorithm (Wang et al., 2021).

3.3 Random Forest (RF) algorithm

The RF algorithm has been extensively investigated by numerous researchers as a technique for classification and regression (Han et al., 2019; Zhang et al., 2019). The concrete compressive strength is predicted by using RF (Shaqadan, 2016). The key distinction between DT and RF lies in the number of trees. While DT builds a single independent tree, RF creates multiple trees, referred to as "forests". Unrelated data are randomly selected and assigned to these trees. Each of these trees comprises columns and rows with data, determining the column and row dimensions. Discrete steps are taken for each tree's growth. This data frame includes two-thirds of randomly selected data for every tree: RF. The prediction variables are selected randomly, and the fine splitting of these variables performs node splitting. In the case of all trees, the lingering data are used to predict the outlier error. Consequently, the ultimate out-of-bag error rate is evaluated by merging errors out of each tree. Every tree offers regression, and the forest with the most votes is adopted from the entire forest. The value of the vote may be 0's and 1's. The attained proportion of 1's stipulates the probability of prediction. RF is an efficient ensemble model, comprising necessary variable importance measures (VIMs) with vigorous resistance against rarer model variables and overfitting. DT is utilized for RF as a base estimator. Satisfactory outcomes may be attained by RF algorithms having variable settings (Xu et al., 2021). RF permits base predictor amalgamations and variable settings to be decreased to 1. The RF step-wise structure is shown in Figure 4.

3.4 Shapley Additive Explanations (SHAP)

This study also uses the SHAP analysis (Lundberg, 2021) to assess the global feature influences and corresponding dependencies/interactions of all selected features on the compressive strength of HSC, thus expanding the model's description. In this technique, the description in the case of estimation for every instance is explained with the help of contribution computations by selected features through SHAP values. The value involvement for each feature against all the probable combinations is averaged to attain the SHAP values. The features with more influence have more definite the SHAP values. The average is taken for the SHAP values of every feature from the dataset to accomplish global feature influences. These values are then sorted in descending order of importance; the plotting is carried out afterward. A unique point in the aforesaid plot shows the SHAP value for individual features and instances. X-axis depicts the SHAP values, whereas feature importance is shown on the y-axis. A higher y-axis value displays a greater feature influence. Furthermore, their significance is illustrated by color scale. SHAP plots of feature dependence demonstrate the feature's interaction and respective effect on the compressive strength of HSC. It can yield improved data compared to partial dependence traditional graphs (Lundberg et al., 2020). In this SHAP analysis, particularly the feature importance "j" against the algorithm's output f; $\phi^j(f)$ is allocated weight to sum the involvement of features for the model output, $f(x_i)$, to attain

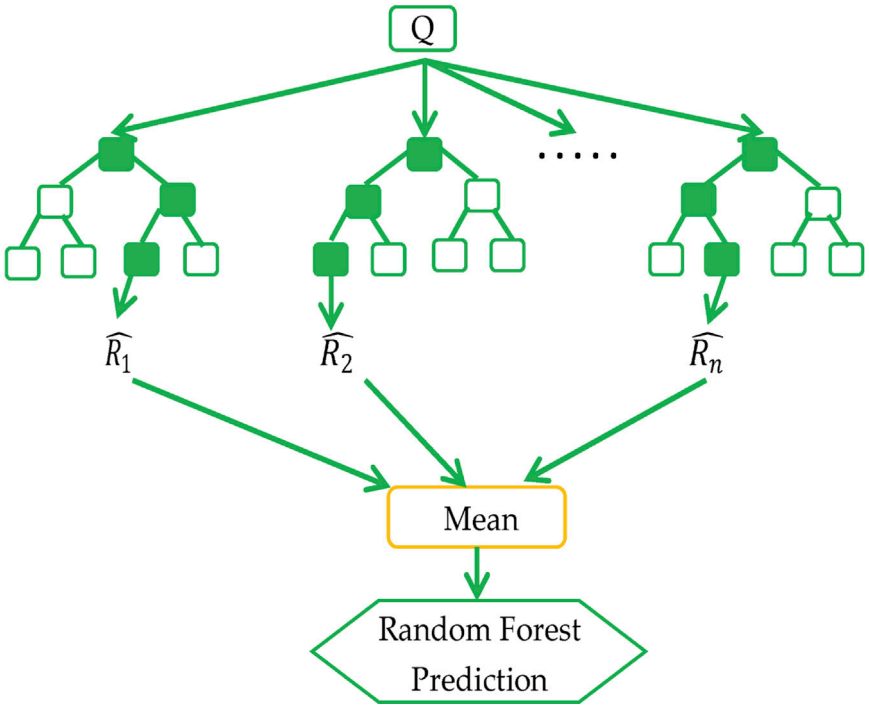

FIGURE 4
Structure of the Random Forest algorithm (Amjad et al., 2022).

the possible combinations of overall features (Molnar, 2020). $\phi^j(f)$ is devised by Eq. 5.

$$\phi^j(f) = \sum_{S \subseteq \{x^1,\ldots,x^p\}/\{x^j\}} \frac{|S|!\,(p-|S|-1)!}{p!} \left(f\left(S \sqcup \{x^j\}\right) - f(S)\right) \tag{5}$$

where x_j = feature j, p = feature number in model, and S = feature subset. The SHAP method employed in this study determines the feature importance by quantifying estimation errors when a particular value of the feature is perturbed. The weight allocation to a feature during the value dispersion is based on the sensitivity of the prediction error. The performance of trained ML algorithms is described through the SHAP analysis. It applies a supplementary feature attribution approach (linear input parameter summation) to illustrate an interpretable algorithm. An algorithm with input variables x_i; i ranges between 1–k; k shows input variables quantity and h (x_s) depicts a descriptive algorithm having x_s in the form of simple input. Eq. 6 is proposed for depicting a unique algorithm $f(x)$.

$$f(x) = h(x_s) = \varnothing_0 + \sum_{i=1}^{p} \varnothing_i x_s^i \tag{6}$$

where $\varnothing_0$ = constant with no information (means no input); p = the number of input features; $x = m_x(x_s)$ indicates a connection between both x and x_s input variables. Lundberg and Lee (2017) proposed Eq. 6, where the prediction value $h()$ was increased by $\varnothing_0, \varnothing_1$, and $\varnothing_3$ relations along with decreased $\varnothing_4$ in the form of $h()$ value, which were also reported in Figure 5. The solution to Eq. 6, which is a single value, incorporates three essential characteristics: missingness, consistency, and local accuracy. The attribution is confirmed by consistency without decrement, assigned to the particular feature having more influence. In the case of missingness, this certifies that there is no importance value which is allocated to missing features—represented by $\varnothing_i = 0$ applied through $x_s^i = 0$. Regarding local accuracy, the feature attribution summation is verified as an output function. This necessitates the use of an algorithm for a similar outcome f for x_s, which serves as a simplified input. $x = m_x x_s$ signifies the local accuracy attainment.

4 Dataset description

The database is developed from the literature (Fu et al., 2005; Cülfik and Özturan, 2010; Ergün et al., 2013; Bastami et al., 2014; Chen et al., 2015; Xiong et al., 2016; Mousa, 2017). For predicting the compressive strength of HSC, the considered input dataset is presented in Figure 6. The available literature was used to obtain data on the compressive strength of HSC, which were then compiled into a database. The input parameters are cement (kg/m^3), fly ash (kg/m^3), nano-silica (kg/m^3), water (kg/m^3), super plasticizer (kg/m^3), fine aggregates (kg/m^3), coarse aggregates (kg/m^3), silica fume (kg/m^3), and temperature (°C) (Figure 6); these parameters are taken as predictor variables for the compressive strength of HSC. This strength is predicted by applying Anaconda Software's Python and Spyder Scripting. Figure 7 illustrates the relative frequency dispersion of the output parameter, i.e., the compressive strength.

5 Results and analysis

5.1 Extreme Gradient Boosting (XGBoost)

Figure 8 displays a comparison between the experimental and predicted values of the compressive strength of HSC using XGBoost, which depicts the highly precise prediction of the compressive strength of HSC. The R^2 value of 0.94 is within a reasonable range, indicating the adequacy of XGBoost. Figure 9 shows the error distribution for the compressive strength of HSC utilizing XGBoost between the estimated and experimental values. The error of the compressive strength of HSC is 4.65 MPa on average. Around 61.2% of the values are below 5 MPa, while there is a 35.48% range from 5 to 10 MPa, with only 3.22% exceeding 10 MPa.

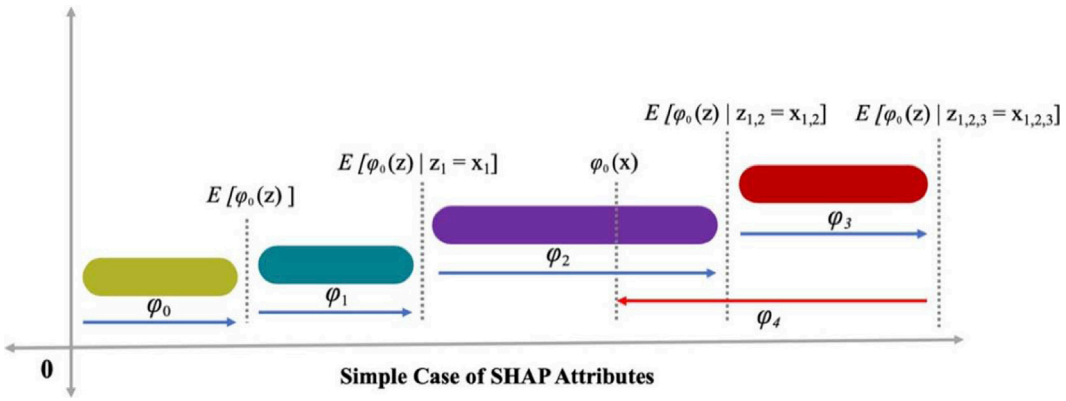

FIGURE 5
Attributes of SHAP (Shen et al., 2022).

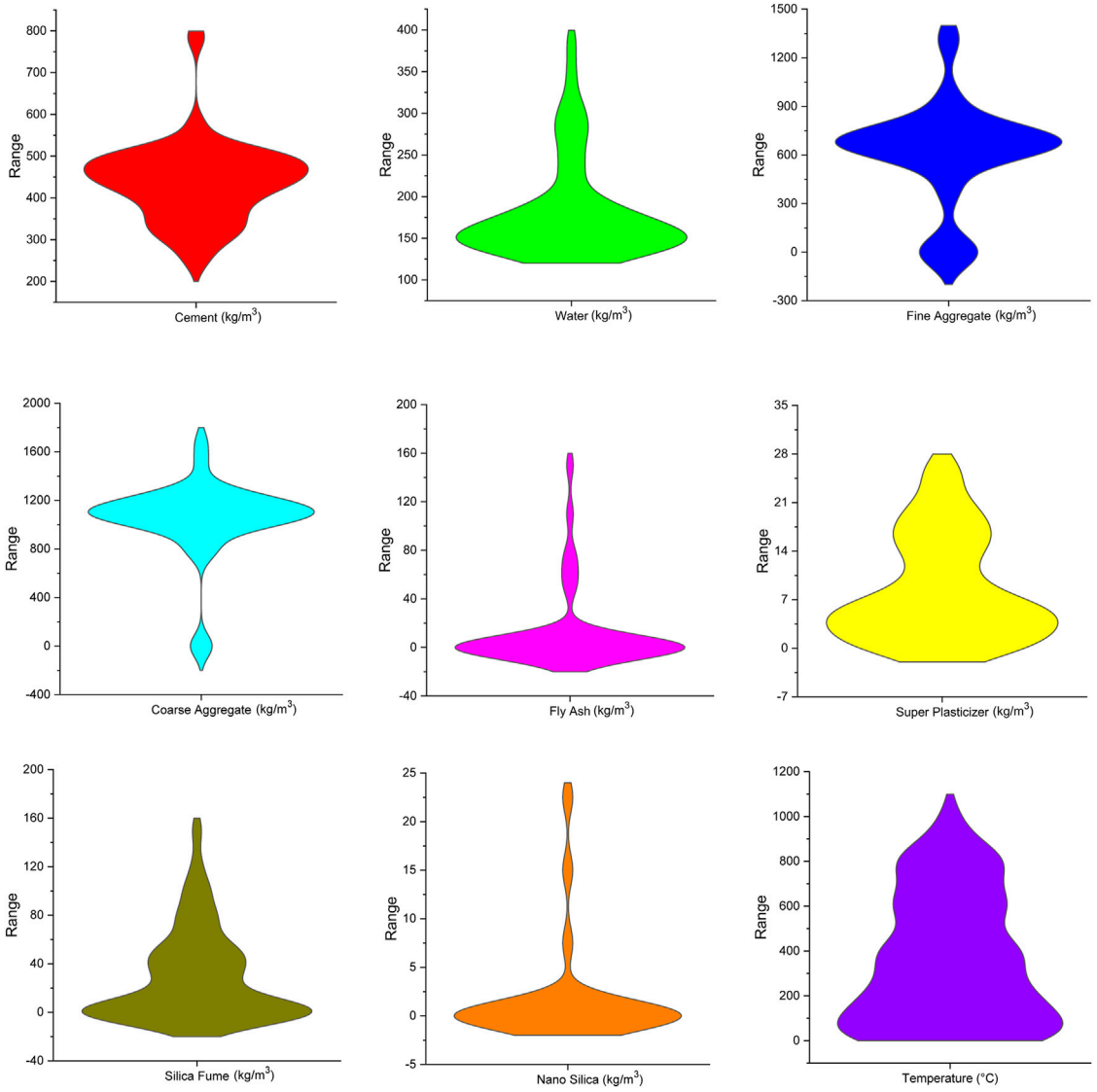

FIGURE 6
Input data parameter description.

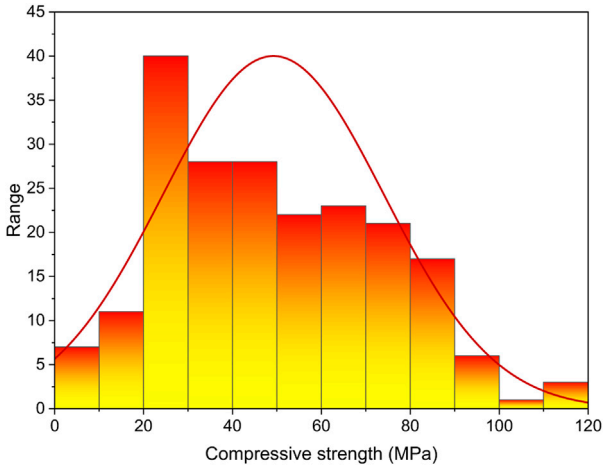

FIGURE 7
Distribution of the compressive strength of HSC.

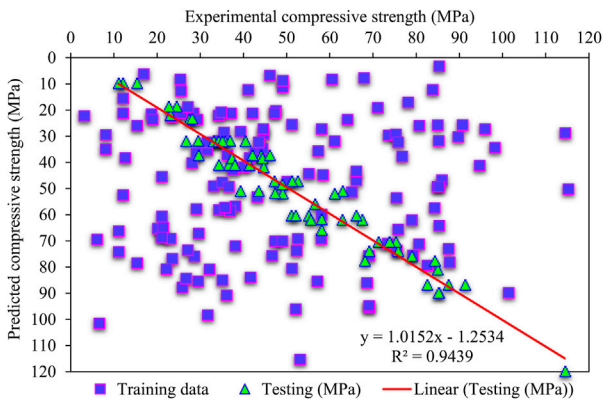

FIGURE 8
XGBoost predicted and experimental results.

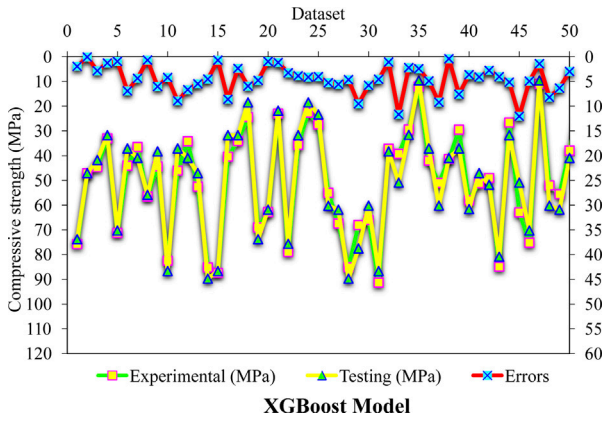

FIGURE 9
XGBoost estimated and experimental values distribution with errors.

Moreover, further statistics such as highest, mean, median, lowest, first, and third quartile values in the case of experimental and predicted results from the test database are demonstrated in Figure 10. It can be seen in the graphical data that there is a difference between predicted and actual outcomes. Based on the box plot, it appears that the median of the actual values is 51.34 MPa, while the median of the predicted values is 50.86 MPa. The fact that these two values are close suggests that the model can predict the target variable relatively accurately.

5.2 Adaptive Boosting (Adaboost)

Figure 11 provides the predicted and actual values for the compressive strength of HSC utilizing the Adaboost algorithm, in which the R^2 value of 0.90 depicts results with comparatively more precision than XGBoost. The error distribution for experimental and Adaboost-predicted values in the case of the compressive strength of HSC is presented in Figure 12. Here, 59.67% of values lie below 5 MPa, 17.74% lie in the range 5–10 MPa, and 22.58% are

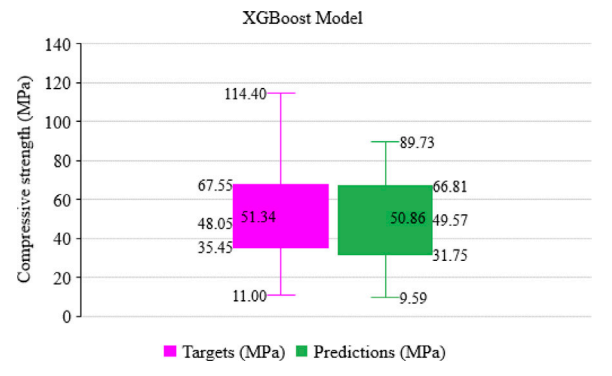

FIGURE 10
Box plot for actual and XGBoost predicted results.

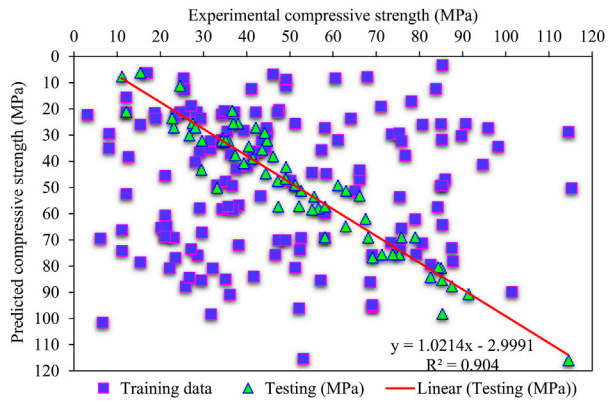

FIGURE 11
Adaboost predicted and experimental results.

above 10 MPa; the lesser R^2 and greater error value represent the poorer accuracy of Adaboost than that of XGBoost.

The box plot (Figure 13) shows the statistical evaluation, such as minimum, mean, maximum, median, and first and third quartile values, for estimated and experimental outcomes from the test database. The box plot indicates that the median value of the actual data is 51.34 MPa, whereas the predicted data have a median of 49.44 MPa. The close proximity of these two median values implies that the model makes relatively accurate predictions of the target variable. One can observe the variance between the anticipated and factual outcomes by examining the numerical values on the graph. It may be noted from the graph data that there is more difference between predicted and actual outcomes than in XGBoost.

5.3 Random Forest (RF)

Figure 14 illustrates the experimental and RF-estimated values regarding the compressive strength of HSC. The R^2 value of 0.98 for RF depicts comparatively more accurate outcomes than the other models considered. Furthermore, the predicted results for the compressive strength of HSC for RF are precise out of the ensemble models employed. Figure 15 presents the dispersal among RF-estimated and experimental outcomes and error values for the compressive strength of HSC. Notably, 95.16% of the entire error values are below 5 MPa, and 4.83% of remaining values are from 5–10 MPa; notably, no value is above 10 MPa. The higher R^2 values of the RF algorithm for the compressive strength of HSC demonstrates better accuracy. Thus, more accurate prediction results can be achieved by utilizing RF than the other models.

In addition, Figure 16 displays the statistical analysis in the form of a box plot, which exhibits the minimum, mean, median, maximum, first quartile, and third quartile values for both the actual and RF-predicted values. According to the box plot, the median value for the actual dataset is 51.34 MPa, while the median value for the predicted dataset is 51.89 MPa. This suggests that the model performs reasonably well in predicting the target variable, as the difference between the two median values is small. The output for the RF model in the case of predicted and actual values is closer, unlike XGBoost and Adaboost.

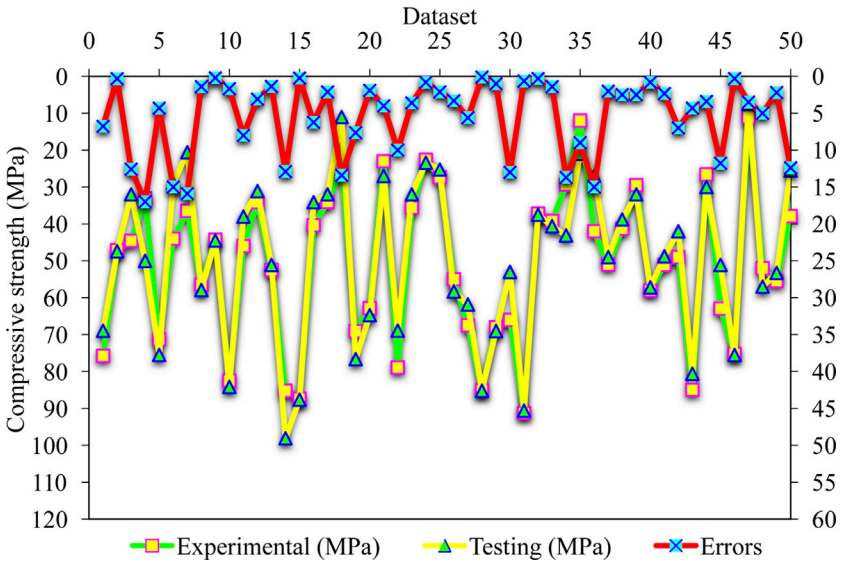

FIGURE 12
Adaboost estimated and experimental values distribution with errors.

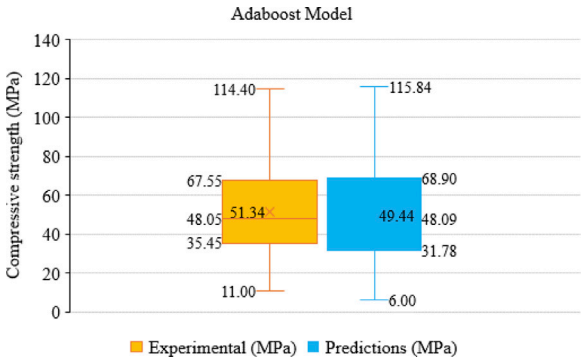

FIGURE 13
Box plot for Adaboost predicted and actual results.

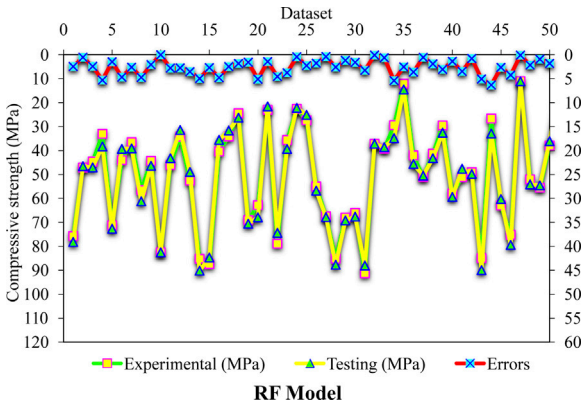

FIGURE 15
RF estimated and experimental values distribution with errors.

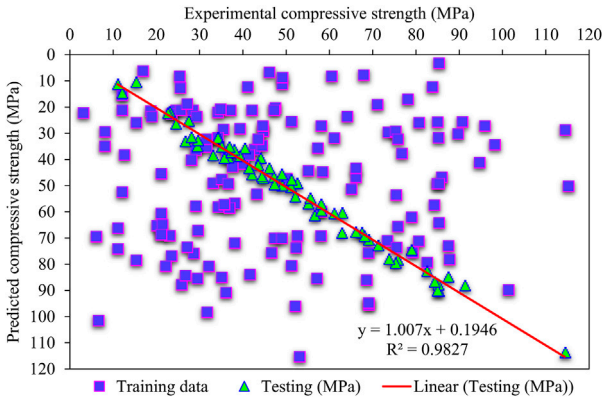

FIGURE 14
RF predicted and experimental results.

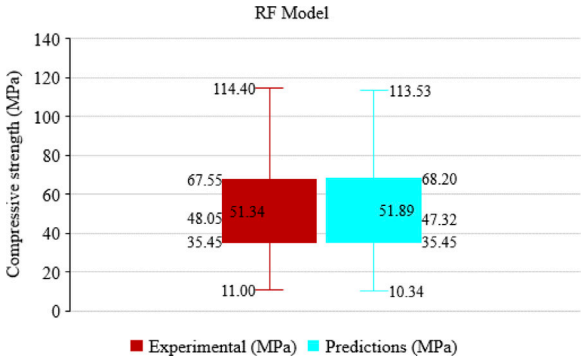

FIGURE 16
Box plot for actual and RF predicted results.

TABLE 1 Statistical analysis for XGBoost, Adaboost, and RF algorithms.

Statistical checks	Techniques		
	XGBoost	Adaboost	RF
R^2	0.94	0.90	0.98
MAE (MPa)	4.7	5.7	2.5
RMSE (MPa)	5.4	7.5	3.0

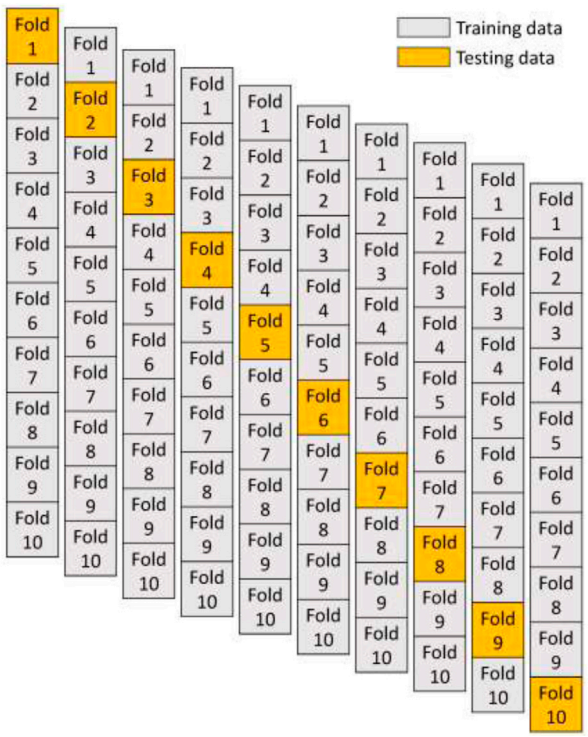

FIGURE 17
K-fold cross-validation procedure (Zou et al., 2022).

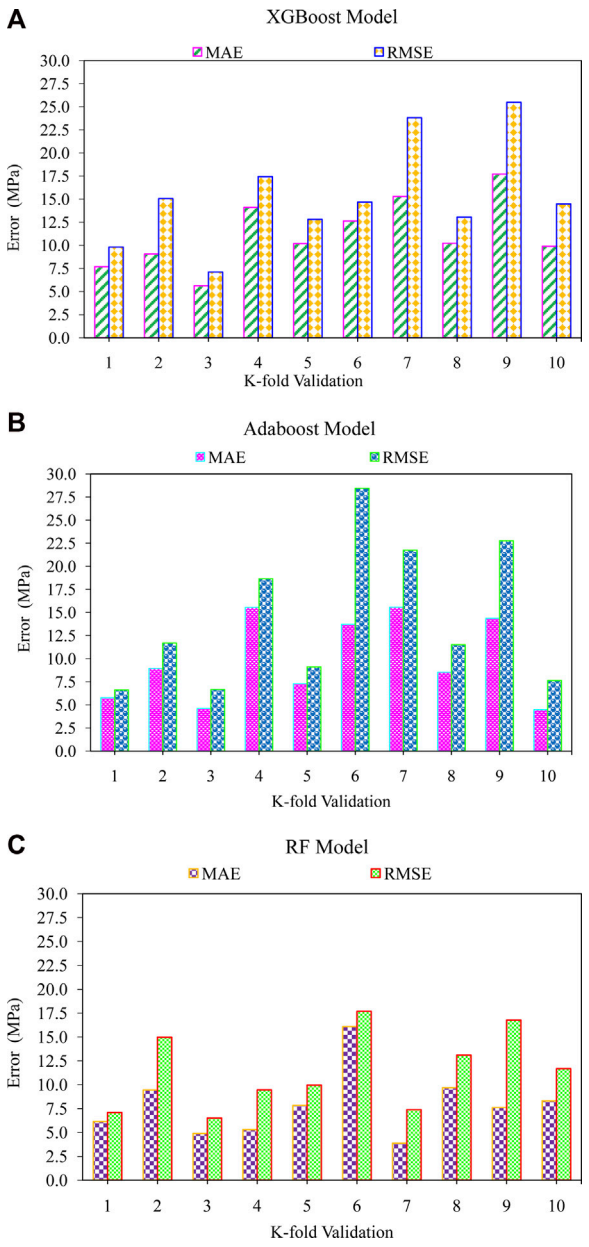

FIGURE 18
Statistical analysis: **(A)** XGBoost; **(B)** Adaboost; **(C)** RF.

5.4 Comparison of models

This study employs the k-fold approach to validate the implemented algorithm. In the literature (Amin et al., 2022a; Khan et al., 2022a; 2022b; Zou et al., 2022), the statistical analysis is reported to assess the model's performance. Usually, data splitting into ten subgroups is carried out for the random dispersion to perform the k-fold process for cross-validation; this approach is repeated ten times to achieve outcomes in a satisfactory range, as shown in Figure 17. Table 1 presents the statistical checks of all the used algorithms. For RF, the R^2 value is 0.98; in Adaboost, the R^2 value is 0.90; for XGBoost, it is 0.94 (Figures 18A–C). The R^2 value for the RF model is higher with lower error values compared to the other considered algorithms to estimate the compressive strength of HSC.

The compressive strength of HSC is predicted by applying ensemble ML techniques in the current work for reliable and efficient outcomes. The R^2 value of RF as 0.98 depicts a more accurate prediction for the compressive strength of HSC. Figures 19A–C show the RF model's superiority for predicting the compressive strength of HSC using a single optimized algorithm from 20 sub-models. Hence, it is concluded that RF has more accuracy and less error than all other algorithms.

5.5 Improved machine learning models' explainability

The current research work indicates an enhanced explanation of the ML algorithms employed along with the interactions of input

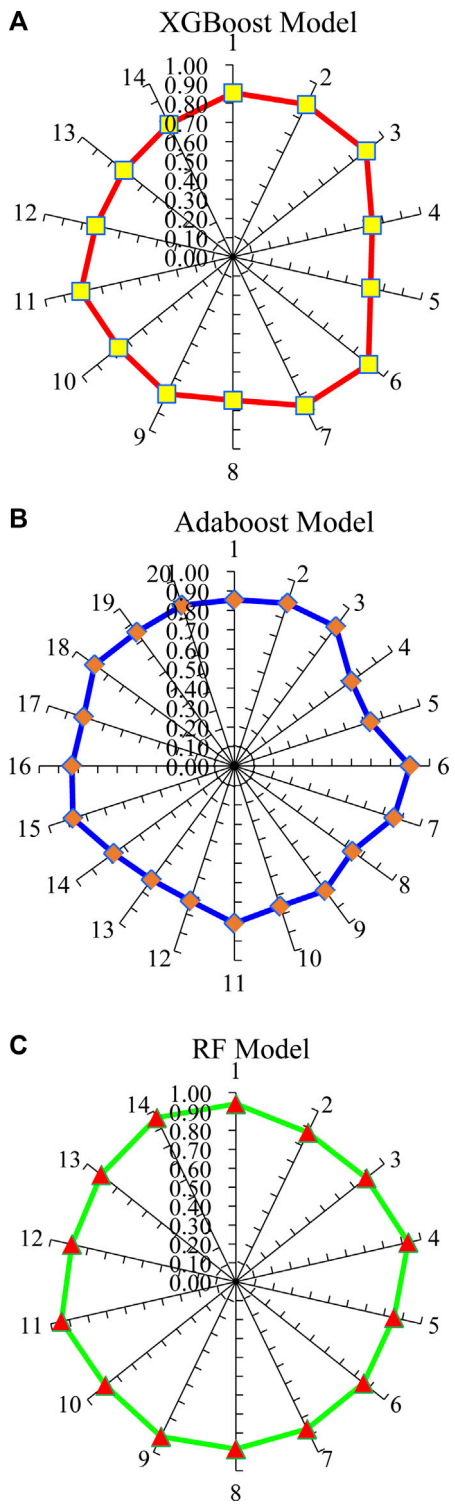

FIGURE 19
Results of sub-models: **(A)** XGBoost; **(B)** Adaboost; **(C)** RF.

features. The SHAP analysis on the entire dataset presents an improved feature that influences global representation due to mergence with local SHAP explanations. The RF algorithm offers the most accurate prediction for the compressive strength of HSC, so here the algorithm is demonstrated for the compressive strength of HSC through the SHAP analysis. The correlation of features with the SHAP values for the strength of HSC is presented in Figure 20. It is notable that the temperature feature is extremely higher in terms of the SHAP values. This depicts that temperature significantly influences the compressive strength of HSC. Increased temperature tends to cause a reduction in the compressive strength. Fine and coarse aggregates also considerably influence the compressive strength of HSC, followed by temperature. As the greater quantity of aggregates offers more matrix interface, this loses its bonding upon heating, resulting in shrinkage cracks and ultimately reducing the compressive strength. Afterward, there is a cement feature which positively influences the compressive strength of HSC. Increasing cement content will thus enhance the compressive strength of HSC. Water indirectly influences the compressive strength of HSC. The strength of the composite is reduced due to a higher water–cement ratio and increased pore water pressure, resulting in excessive cracking and explosive spalling. Increased water content would result in decreased strength of HSC. Fly ash positively influences the strength of HSC as further hydration is achieved. Similarly, super plasticizers, silica fume, and nano-silica also have slight but positive influences on the compressive strength of HSC.

The interaction of the features with the compressive strength of HSC is illustrated in Figure 21. Figure 21A depicts the cement feature interaction, which directly influences the strength of HSC. The negative influence of water is observed for the compressive strength of HSC (Figure 21B). In this case, the inverse relation with the compressive strength of HSC is noted. The fine aggregate feature dependency is shown in Figure 21C: the impact of fine aggregates on silica fume also demonstrates a negative influence, resulting in decreased compressive strength of HSC. Thereafter, both positive and negative influences are witnessed in the coarse aggregate feature and are dependent on content (Figure 21D). Therefore, up to optimal content, coarse aggregates would contribute to the compressive strength of HSC and thence reduce the strength. The fly ash, super plasticizer, and silica fume interaction plots are presented in Figures 21E–G. In these three plots, the direct/positive influence of all said features is depicted for the compressive strength of HSC. However, in the case of the temperature feature plot (Figure 21H), an inverse relation of temperature is reported with the compressive strength of HSC.

6 Discussion

The use of advanced predictive modeling techniques has become significantly popular in recent years (Chen et al., 2022; Wang et al., 2022; Amin et al., 2023; Nazar et al., 2023a; 2023b). Numerous studies have employed ML algorithms such as Gene Expression Programming, Bagging Regressor, AdaBoost, and RF to predict the compressive, splitting-tensile, and shear strengths of various composites, including geopolymer concrete, recycled aggregate concrete, ultra-high-performance concrete, and rice husk ash concrete. Table 2 summarizes these studies, highlighting the ML algorithms used and the properties predicted for various cementitious composites. The comparison allows for an assessment of the efficiency and reliability of the algorithms employed in this study compared to other literature

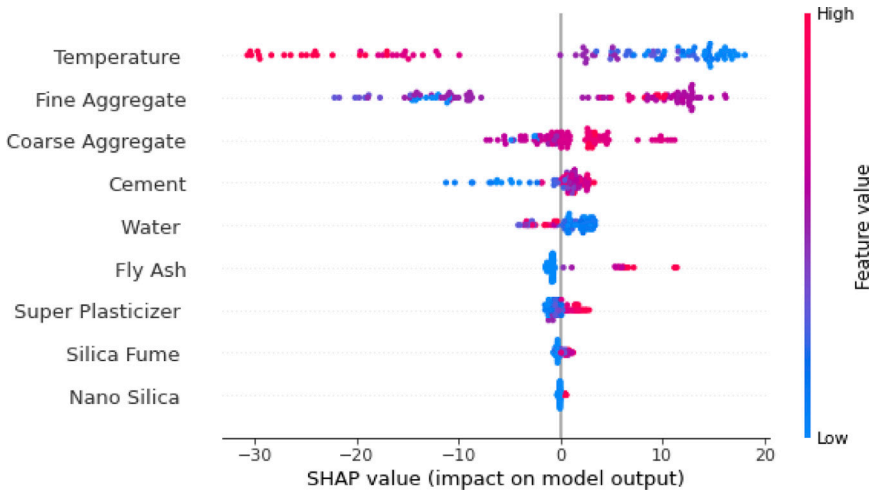

FIGURE 20
SHAP plot.

studies. The RF model in this study produces the R^2 value of 0.98, indicating a high level of precision in predicting the compressive strength of HSC. Overall, Table 2 signifies that the RF model provides relatively accurate predictions, consistent with the literature. It is worth noting that, after RF, the XGBoost and GB algorithms exhibit greater precision than the other algorithms. In our study, XGBoost also performed well after RF, with the R^2 value of 0.94, and AdaBoost demonstrated the acceptable R^2 value of 0.90. Thus, the use of ML algorithms indicates significant potential for predicting the mechanical properties of various cementitious composites. The results of this study demonstrate the effectiveness of the RF, XGBoost, and AdaBoost algorithms in predicting the compressive strength of HSC, with RF showing the highest level of precision. These findings suggest that ML techniques can be a valuable tool in the field of concrete, offering a reliable and efficient method for predicting the properties of HSC.

7 Conclusion

In the construction industry, the utilization of ML methodologies is increasingly recognized as a promising approach for predicting the concrete's mechanical characteristics. The current study's primary aim is to assess the precision of ML techniques to estimate the compressive strength of HSC at elevated temperatures. To predict the compressive strength of HSC using ML algorithms, various input parameters are considered predictor variables. The following points are concluded.

- The R^2 value of 0.98 for the RF algorithm depicts its precision in predicting the compressive strength of HSC. However, in ensemble XGBoost and Adaboost ML algorithms, the R^2 values are 0.94 and 0.90, respectively, showing lesser accuracy in predicting the compressive strength of HSC.
- By utilizing 20 sub-algorithms within a range of 10–200 estimates, the optimal compressive strength of HSC is predicted. The RF ensemble model is comparatively more accurate in predicting the compressive strength of HSC than the other algorithms considered.
- It is revealed from the k-fold test results that the RF and XGBoost algorithms show lesser RMSE and MAE values and greater R^2 values in case of the compressive strength of HSC than the other algorithms. At the same time, RF has the highest prediction accuracy to predict the strength of HSC.
- The efficiency of the models employed is also assessed with the help of statistical measures such as MAE and RMSE. Higher coefficient of determination values and lower error values indicate that RF is more accurate than XGBoost and AdaBoost in predicting the compressive strength of HSC.
- From all the applied ML approaches, RF is the most accurate approach for precise prediction of the compressive strength of HSC.
- According to the SHAP analysis, temperature features have the greatest impact on the strength of HSC, followed by the contributions of fine and coarse aggregates, cement, water, fly ash, super plasticizer, and silica fume. However, nano-silica has the least influence on the prediction of the compressive strength of HSC.
- The compressive strength of HSC is positively and negatively affected by cement and temperature, respectively, as extracted from the feature interaction plot.
- Further investigation is required to examine the load–slip modeling of HSC, specifically regarding the age of the matrix and strength.

To improve the effectiveness of HSC modeling with respect to the age of the matrix and strength, future studies could focus

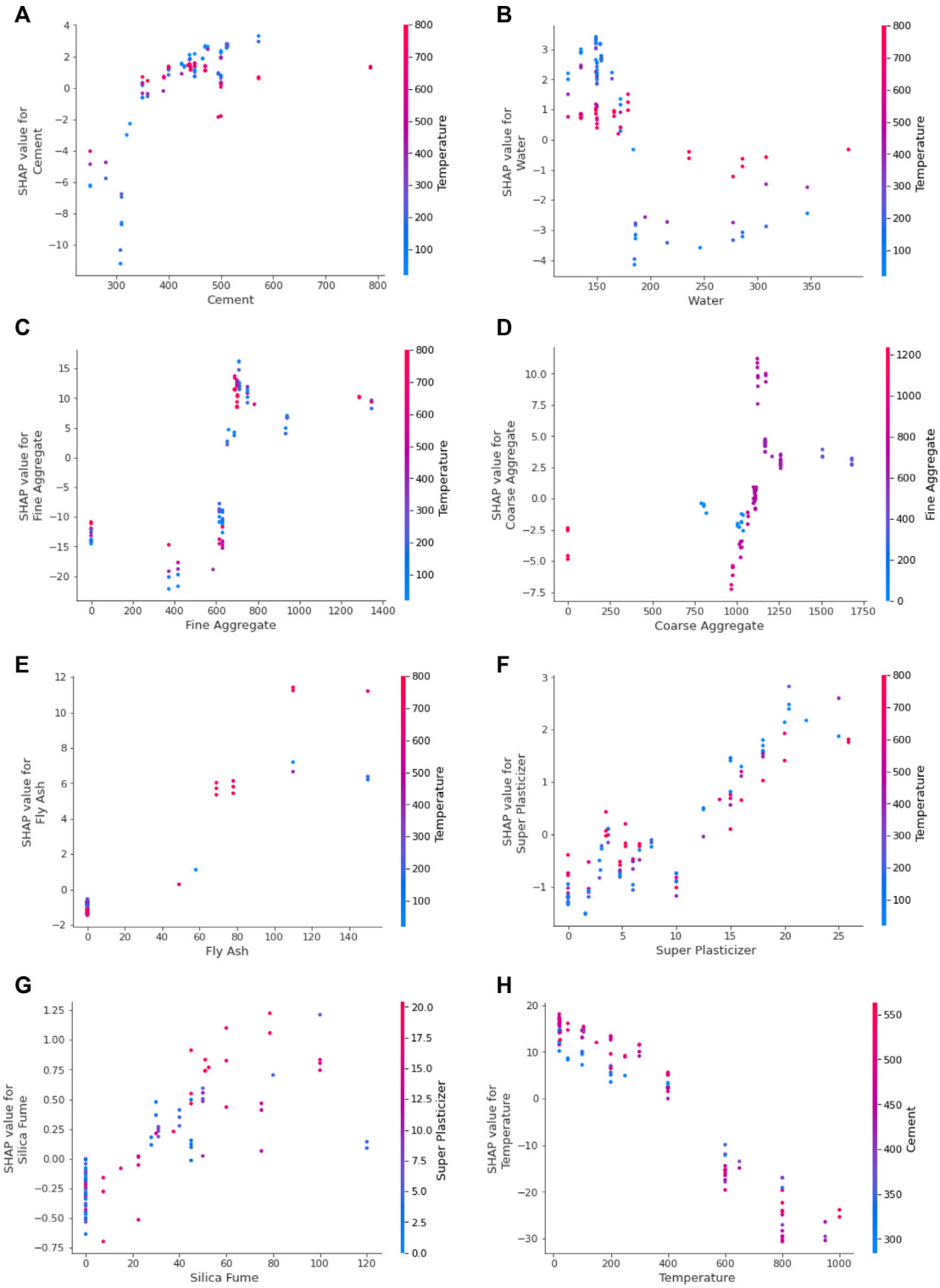

FIGURE 21
Feature interaction plot: **(A)** cement, **(B)** water, **(C)** fine aggregate, **(D)** coarse aggregate, **(E)** fly ash, **(F)** super plasticizer, **(G)** silica fume, and **(H)** temperature.

on employing deep learning algorithms due to their ability to handle complex and non-linear relationships. Additionally, the use of deep learning in conjunction with metaheuristic optimization techniques can further increase the accuracy of predictions and enhance the overall modeling process. It is also recommended that a larger and more comprehensive dataset be

TABLE 2 Summary of prediction models in the current study and in the literature.

References	Material description	ML approaches	R^2
Current study	High-strength concrete (HSC)	Random Forest (RF)	0.98
Current study	High-strength concrete (HSC)	Extreme Gradient Bosting (XGBoost)	0.94
Current study	High-strength concrete (HSC)	Adaptive Boosting (Adaboost)	0.90
Ahmad et al. (2021)	High-strength concrete (HSC)	Decision Tree (DT)	0.83
Ahmad et al. (2021)	High-strength concrete (HSC)	Artificial Neural Network (ANN)	0.82
Zou et al. (2022)	Geopolymer concrete	Decision Tree (DT)	0.88
Ahmad et al. (2021)	Fly ash concrete	Decision Tree (DT)	0.83
Khan et al. (2022b)	Waste marble powder concrete (WMC)	Adaptive Boosting (AdaBoost)	0.91
Amin et al. (2022a)	Recycled coarse aggregate concrete (RCAC)	Gradient Bosting (GB)	0.94
Khan et al. (2022a)	Fly ash concrete	Bootstrap Aggregation (BA)	0.93
Amin et al. (2022b)	Geopolymer concrete	Multiple Layer Perceptron Neural Network (MLPNN)	0.81
Amin et al. (2022b)	Geopolymer concrete	Support Vector Machine (SVM)	0.78

utilized to train and test the deep learning models to achieve better results.

Data availability statement

The original contributions presented in the study are included in the article/Supplementary material; further inquiries can be directed to the corresponding authors.

Author contributions

GC: conceptualization, methodology, resources, writing—original draft, and project administration. SS: investigation, software, methodology, and writing—review and editing. AB: conceptualization, methodology, investigation, software, validation, formal analysis, resources, writing—original draft, writing—review and editing, and project administration. MS: methodology, investigation, validation, and writing—review and editing. MA: validation, formal analysis, resources, and writing—review and editing.

Conflict of interest

The authors declare that the research was conducted in the absence of any commercial or financial relationships that could be construed as a potential conflict of interest.

Publisher's note

References

Afzal, M. T., and Khushnood, R. A. (2021). Influence of carbon nano fibers (CNF) on the performance of high strength concrete exposed to elevated temperatures. *Constr. Build. Mater.* 268, 121108. doi:10.1016/j.conbuildmat.2020.121108

Ahmad, A., Ostrowski, K. A., Maślak, M., Farooq, F., Mehmood, I., and Nafees, A. (2021). Comparative study of supervised machine learning algorithms for predicting the compressive strength of concrete at high temperature. *Materials* 14, 4222. doi:10.3390/ma14154222

Ahmad, M. R., Das, C. S., Khan, M., and Dai, J.-G. (2023). Development of low-carbon alkali-activated materials solely activated by flue gas residues (FGR) waste from incineration plants. *J. Clean. Prod.* 397, 136597. doi:10.1016/j.jclepro.2023.136597

Alfahdawi, I. H., Osman, S., Hamid, R., and Al-Hadithi, A. I. (2019). Influence of PET wastes on the environment and high strength concrete properties exposed to high temperatures. *Constr. Build. Mater.* 225, 358–370. doi:10.1016/j.conbuildmat.2019.07.214

Al-Shamiri, A. K., Kim, J. H., Yuan, T.-F., and Yoon, Y. S. (2019). Modeling the compressive strength of high-strength concrete: An extreme learning approach. *Constr. Build. Mater.* 208, 204–219. doi:10.1016/j.conbuildmat.2019.02.165

Amin, M. N., Ahmad, W., Khan, K., Ahmad, A., Nazar, S., and Alabdullah, A. A. (2022a). Use of artificial intelligence for predicting parameters of sustainable concrete and raw ingredient effects and interactions. *Materials* 15, 5207. doi:10.3390/ma15155207

Amin, M. N., Khan, K., Ahmad, W., Javed, M. F., Qureshi, H. J., Saleem, M. U., et al. (2022b). Compressive strength estimation of geopolymer composites through novel computational approaches. *Polymers* 14, 2128. doi:10.3390/polym14102128

Amin, M. N., Iftikhar, B., Khan, K., Javed, M. F., Abuarab, A. M., and Rehman, M. F. (2023). Prediction model for rice husk ash concrete using AI approach: Boosting and bagging algorithms. *Structures* 50, 745–757. doi:10.1016/j.istruc.2023.02.080

Amjad, M., Ahmad, I., Ahmad, M., Wróblewski, P., Kamiński, P., and Amjad, U. (2022). Prediction of pile bearing capacity using XGBoost algorithm: Modeling and performance evaluation. *Appl. Sci.* 12, 2126. doi:10.3390/app12042126

Arshad, S., Sharif, M. B., Irfan-Ul-Hassan, M., Khan, M., and Zhang, J.-L. (2020). Efficiency of supplementary cementitious materials and natural fiber on mechanical performance of concrete. *Arabian J. Sci. Eng.* 45, 8577–8589. doi:10.1007/s13369-020-04769-z

Asghari, Y., Sadeghian, G., Mohammadyan-Yasouj, S. E., and Mirzaei, E. (2023). Forecast of modern concrete properties using machine learning methods, *Artificial intelligence in mechatronics and civil engineering: Bridging the gap*, 167–205.

Bastami, M., Baghbadrani, M., and Aslani, F. (2014). Performance of nano-silica modified high strength concrete at elevated temperatures. *Constr. Build. Mater.* 68, 402–408. doi:10.1016/j.conbuildmat.2014.06.026

Bilodeau, A., Kodur, V., and Hoff, G. (2004). Optimization of the type and amount of polypropylene fibres for preventing the spalling of lightweight concrete subjected to hydrocarbon fire. *Cem. Concr. Compos.* 26, 163–174. doi:10.1016/s0958-9465(03)00085-4

Cao, M., Mao, Y., Khan, M., Si, W., and Shen, S. (2018). Different testing methods for assessing the synthetic fiber distribution in cement-based composites. *Constr. Build. Mater.* 184, 128–142. doi:10.1016/j.conbuildmat.2018.06.207

Cao, M., Xie, C., Li, L., and Khan, M. (2019). Effect of different PVA and steel fiber length and content on mechanical properties of $CaCO_3$ whisker reinforced cementitious composites. *Mater. Construcción* 69, e200. doi:10.3989/mc.2019.12918

Carrasquillo, R. L., Nilson, A. H., and Slate, F. O. (1981). Properties of high strength concrete subjectto short-term loads. *J. Proc.* 78, 171–178. doi:10.14359/6914

Castelli, M., Vanneschi, L., and Silva, S. (2013). Prediction of high performance concrete strength using genetic programming with geometric semantic genetic operators. *Expert Syst. Appl.* 40, 6856–6862. doi:10.1016/j.eswa.2013.06.037

Chaabene, W. B., Flah, M., and Nehdi, M. L. (2020). Machine learning prediction of mechanical properties of concrete: Critical review. *Constr. Build. Mater.* 260, 119889. doi:10.1016/j.conbuildmat.2020.119889

Chen, T., and Guestrin, C. (2016). "Xgboost: A scalable tree boosting system," in Proceedings of the 22nd acm sigkdd international conference on knowledge discovery and data mining, August 2016, 785–794.

Chen, L., Fang, Q., Jiang, X., Ruan, Z., and Hong, J. (2015). Combined effects of high temperature and high strain rate on normal weight concrete. *Int. J. Impact Eng.* 86, 40–56. doi:10.1016/j.ijimpeng.2015.07.002

Chen, J., Tong, H., Yuan, J., Fang, Y., and Gu, R. (2022). Permeability prediction model modified on kozeny-carman for building foundation of clay soil. *Buildings* 12, 1798. doi:10.3390/buildings12111798

Cülfik, M. S., and Özturan, T. (2010). Mechanical properties of normal and high strength concretes subjected to high temperatures and using image analysis to detect bond deteriorations. *Constr. Build. Mater.* 24, 1486–1493. doi:10.1016/j.conbuildmat.2010.01.020

Dong, H., Linghu, J., and Nie, Y. (2023a). Integrated wavelet-learning method for macroscopic mechanical properties prediction of concrete composites with hierarchical random configurations. *Compos. Struct.* 304, 116357. doi:10.1016/j.compstruct.2022.116357

Dong, Z., Quan, W., Ma, X., Li, X., and Zhou, J. (2023b). Asymptotic homogenization of effective thermal-elastic properties of concrete considering its three-dimensional mesostructure. *Comput. Struct.* 279, 106970. doi:10.1016/j.compstruc.2022.106970

Duan, Z. H., Kou, S. C., and Poon, C. S. (2013). Prediction of compressive strength of recycled aggregate concrete using artificial neural networks. *Constr. Build. Mater.* 40, 1200–1206. doi:10.1016/j.conbuildmat.2012.04.063

Ergün, A., Kürklü, G., Serhat, B. M., and Mansour, M. Y. (2013). The effect of cement dosage on mechanical properties of concrete exposed to high temperatures. *Fire Saf. J.* 55, 160–167. doi:10.1016/j.firesaf.2012.10.016

Friedman, J. H. (2001). Greedy function approximation: A gradient boosting machine. *Ann. statistics* 29, 1189–1232. doi:10.1214/aos/1013203451

Fu, Y., Wong, Y., Poon, C. S., and Tang, C. (2005). Stress–strain behaviour of high-strength concrete at elevated temperatures. *Mag. Concr. Res.* 57, 535–544. doi:10.1680/macr.2005.57.9.535

Han, Q., Gui, C., Xu, J., and Lacidogna, G. (2019). A generalized method to predict the compressive strength of high-performance concrete by improved random forest algorithm. *Constr. Build. Mater.* 226, 734–742. doi:10.1016/j.conbuildmat.2019.07.315

Huang, S., Huang, M., and Lyu, Y. (2021). Seismic performance analysis of a wind turbine with a monopile foundation affected by sea ice based on a simple numerical method. *Eng. Appl. Comput. fluid Mech.* 15, 1113–1133. doi:10.1080/19942060.2021.1939790

Huang, H., Li, M., Yuan, Y., and Bai, H. (2022). Theoretical analysis on the lateral drift of precast concrete frame with replaceable artificial controllable plastic hinges. *J. Build. Eng.* 62, 105386. doi:10.1016/j.jobe.2022.105386

Huang, H., Li, M., Yuan, Y., and Bai, H. (2023a). Experimental research on the seismic performance of precast concrete frame with replaceable artificial controllable plastic hinges. *J. Struct. Eng.* 149, 04022222. doi:10.1061/jsendh.steng-11648

Huang, Y., Huang, J., Zhang, W., and Liu, X. (2023b). Experimental and numerical study of hooked-end steel fiber-reinforced concrete based on the meso-and macro-models. *Compos. Struct.* 309, 116750. doi:10.1016/j.compstruct.2023.116750

Khaliq, W., and Kodur, V. (2018). Effectiveness of polypropylene and steel fibers in enhancing fire resistance of high-strength concrete columns. *J. Struct. Eng.* 144, 04017224. doi:10.1061/(asce)st.1943-541x.0001981

Khan, M., Cao, M., Xie, C., and Ali, M. (2021). Efficiency of basalt fiber length and content on mechanical and microstructural properties of hybrid fiber concrete. *Fatigue and Fract. Eng. Mater. Struct.* 44, 2135–2152. doi:10.1111/ffe.13483

Khan, K., Ahmad, A., Amin, M. N., Ahmad, W., Nazar, S., and Arab, A. M. A. (2022a). Comparative study of experimental and modeling of fly ash-based concrete. *Materials* 15, 3762. doi:10.3390/ma15113762

Khan, K., Ahmad, W., Amin, M. N., Ahmad, A., Nazar, S., Alabdullah, A. A., et al. (2022b). Exploring the use of waste marble powder in concrete and predicting its strength with different advanced algorithms. *Materials* 15, 4108. doi:10.3390/ma15124108

Khan, M., Cao, M., Chaopeng, X., and Ali, M. (2022c). Experimental and analytical study of hybrid fiber reinforced concrete prepared with basalt fiber under high temperature. *Fire Mater.* 46, 205–226. doi:10.1002/fam.2968

Khan, M., Lao, J., and Dai, J.-G. (2022d). Comparative study of advanced computational techniques for estimating the compressive strength of UHPC. *J. Asian Concr. Fed.* 8, 51–68. doi:10.18702/acf.2022.6.8.1.51

Kushnir, A. R., Heap, M. J., Griffiths, L., Wadsworth, F. B., Langella, A., Baud, P., et al. (2021). The fire resistance of high-strength concrete containing natural zeolites. *Cem. Concr. Compos.* 116, 103897. doi:10.1016/j.cemconcomp.2020.103897

Lalu, O., Darmon, R., and Lennon, T. (2021). "Spalling of high strength concrete in fire," in *IOP conference series: Materials science and engineering* (Bristol, England: IOP Publishing), 012027.

Laneyrie, C., Beaucour, A.-L., Green, M. F., Hebert, R. L., Ledesert, B., and Noumowe, A. (2016). Influence of recycled coarse aggregates on normal and high performance concrete subjected to elevated temperatures. *Constr. Build. Mater.* 111, 368–378. doi:10.1016/j.conbuildmat.2016.02.056

Lao, J.-C., Huang, B.-T., Xu, L.-Y., Khan, M., Fang, Y., and Dai, J.-G. (2023a). Seawater sea-sand Engineered Geopolymer Composites (EGC) with high strength and high ductility. *Cem. Concr. Compos.* 138, 104998. doi:10.1016/j.cemconcomp.2023.104998

Lao, J.-C., Xu, L.-Y., Huang, B.-T., Zhu, J.-X., Khan, M., and Dai, J.-G. (2023b). Utilization of sodium carbonate activator in strain-hardening ultra-high-performance geopolymer concrete (SH-uhpgc). *Front. Mater.* 10, 1–12. doi:10.3389/fmats.2023.1142237

Li, L., Khan, M., Bai, C., and Shi, K. (2021). Uniaxial tensile behavior, flexural properties, empirical calculation and microstructure of multi-scale fiber reinforced cement-based material at elevated temperature. *Materials* 14, 1827. doi:10.3390/ma14081827

Lundberg, S. M., and Lee, S.-I. (2017). A unified approach to interpreting model predictions. *Adv. neural Inf. Process. Syst.* 30. Available at: https://arxiv.org/abs/1705.07874.

Lundberg, S. M., Erion, G., Chen, H., Degrave, A., Prutkin, J. M., Nair, B., et al. (2020). From local explanations to global understanding with explainable AI for trees. *Nat. Mach. Intell.* 2, 56–67. doi:10.1038/s42256-019-0138-9

Lundberg, S. (2021). *A game theoretic approach to explain the output of any machine learning model*. San Francisco: Github.

Marani, A., and Nehdi, M. L. (2020). Machine learning prediction of compressive strength for phase change materials integrated cementitious composites. *Constr. Build. Mater.* 265, 120286. doi:10.1016/j.conbuildmat.2020.120286

Molnar, C. (2020). *Interpretable machine learning*. NC, United States: Lulu. com.

Mousa, M. I. (2017). Effect of elevated temperature on the properties of silica fume and recycled rubber-filled high strength concretes (RHSC). *HBRC J.* 13, 1–7. doi:10.1016/j.hbrcj.2015.03.002

Nazar, S., Yang, J., Amin, M. N., Khan, K., Ashraf, M., Aslam, F., et al. (2023a). Machine learning interpretable-prediction models to evaluate the slump and strength of fly ash-based geopolymer. *J. Mater. Res. Technol.* 24, 100–124. doi:10.1016/j.jmrt.2023.02.180

Nazar, S., Yang, J., Javed, M. F., Khan, K., Li, L., and Liu, Q.-F. (2023b). An evolutionary machine learning-based model to estimate the rheological parameters of fresh concrete. *Structures* 48, 1670–1683. doi:10.1016/j.istruc.2023.01.019

Ozawa, M., Sakoi, Y., Fujimoto, K., Tetsura, K., and Parajuli, S. S. (2017). Estimation of chloride diffusion coefficients of high-strength concrete with synthetic fibres after fire exposure. *Constr. Build. Mater.* 143, 322–329. doi:10.1016/j.conbuildmat.2017.03.117

Qian, L.-P., Ahmad, M. R., Lao, J.-C., and Dai, J.-G. (2023). Recycling of red mud and flue gas residues in geopolymer aggregates (GPA) for sustainable concrete. *Resour. Conservation Recycl.* 191, 106893. doi:10.1016/j.resconrec.2023.106893

Ramadan Suleiman, A., and Nehdi, M. L. (2017). Modeling self-healing of concrete using hybrid genetic algorithm–artificial neural network. *Materials* 10, 135. doi:10.3390/ma10020135

Riaz Ahmad, M., Khan, M., Wang, A., Zhang, Z., and Dai, J.-G. (2023). Alkali-activated materials partially activated using flue gas residues: An insight into reaction products. *Constr. Build. Mater.* 371, 130760. doi:10.1016/j.conbuildmat.2023.130760

Sami, B. H. Z., Sami, B. F. Z., Kumar, P., Ahmed, A. N., Amieghemen, G. E., Sherif, M. M., et al. (2023). Feasibility analysis for predicting the compressive and tensile strength of concrete using machine learning algorithms. *Case Stud. Constr. Mater.* 18, e01893. doi:10.1016/j.cscm.2023.e01893

Shaqadan, A. (2016). Prediction of concrete mix strength using random forest model. *Int. J. Appl. Eng. Res.* 11, 11024–11029.

Shen, Z., Deifalla, A. F., Kamiński, P., and Dyczko, A. (2022). Compressive strength evaluation of ultra-high-strength concrete by machine learning. *Materials* 15, 3523. doi:10.3390/ma15103523

Shi, T., Liu, Y., Hu, Z., Cen, M., Zeng, C., Xu, J., et al. (2022). Deformation performance and fracture toughness of carbon nanofiber-modified cement-based materials. *ACI Mater. J.* 119.

Sun, L., Wang, C., Zhang, C., Yang, Z., Li, C., and Qiao, P. (2023). Experimental investigation on the bond performance of sea sand coral concrete with FRP bar reinforcement for marine environments. *Adv. Struct. Eng.* 26, 533–546. doi:10.1177/13694332221131153

Wang, C., Xu, S., and Yang, J. (2021). Adaboost algorithm in artificial intelligence for optimizing the IRI prediction accuracy of asphalt concrete pavement. *Sensors* 21, 5682. doi:10.3390/s21175682

Wang, Q., Hussain, A., Farooqi, M. U., and Deifalla, A. F. (2022). Artificial intelligence-based estimation of ultra-high-strength concrete's flexural property. *Case Stud. Constr. Mater.* 17, e01243. doi:10.1016/j.cscm.2022.e01243

Wróblewski, R., and Stawiski, B. (2020). Ultrasonic assessment of the concrete residual strength after a real fire exposure. *Buildings* 10, 154. doi:10.3390/buildings10090154

Xie, C., Cao, M., Khan, M., Yin, H., and Guan, J. (2021). Review on different testing methods and factors affecting fracture properties of fiber reinforced cementitious composites. *Constr. Build. Mater.* 273, 121766. doi:10.1016/j.conbuildmat.2020.121766

Xiong, M.-X., and Liew, J. R. (2020). Buckling behavior of circular steel tubes infilled with C170/185 ultra-high-strength concrete under fire. *Eng. Struct.* 212, 110523. doi:10.1016/j.engstruct.2020.110523

Xiong, Y., Deng, S., and Wu, D. (2016). Experimental study on compressive strength recovery effect of fire-damaged high strength concrete after realkalisation treatment. *Procedia Eng.* 135, 476–481. doi:10.1016/j.proeng.2016.01.158

Xu, Y., Ahmad, W., Ahmad, A., Ostrowski, K. A., Dudek, M., Aslam, F., et al. (2021). Computation of high-performance concrete compressive strength using standalone and ensembled machine learning techniques. *Materials* 14, 7034. doi:10.3390/ma14227034

Zhang, J., Ma, G., Huang, Y., Aslani, F., and Nener, B. (2019). Modelling uniaxial compressive strength of lightweight self-compacting concrete using random forest regression. *Constr. Build. Mater.* 210, 713–719. doi:10.1016/j.conbuildmat.2019.03.189

Zhang, J., Huang, Y., Aslani, F., Ma, G., and Nener, B. (2020). A hybrid intelligent system for designing optimal proportions of recycled aggregate concrete. *J. Clean. Prod.* 273, 122922. doi:10.1016/j.jclepro.2020.122922

Zhang, C., Yin, Y., Yan, H., Zhu, S., Li, B., Hou, X., et al. (2023). Centrifuge modeling of multi-row stabilizing piles reinforced reservoir landslide with different row spacings. *Landslides* 20, 559–577. doi:10.1007/s10346-022-01994-5

Zou, Y., Zheng, C., Alzahrani, A. M., Ahmad, W., Ahmad, A., Mohamed, A. M., et al. (2022). Evaluation of artificial intelligence methods to estimate the compressive strength of geopolymers. *Gels* 8, 271. doi:10.3390/gels8050271